timsTOF Pro

The New Standard for Shotgun Proteomics

BRUKER

Powered by PASEF

While delivering revolutionary improvements in speed, specificity and sensitivity, the timsTOF Pro with TIMS-based PASEF technology also delivers accurate CCS values for all peptides separated in the ion mobility dimension. By doing so, it ushers in the era of 4D-Proteomics and gives scientists the tools to dig deeper into the complex biology revealed by the deep proteome.

- Near 100% duty cycle using dual TIMS technology
- Unrivalled MS/MS speed >100Hz
- Discover more proteins using PASEF

For more information please visit www.bruker.com/timstofpro

TIMS-QTOF MS

Innovation with Integrity

Proteomics
www.proteomics-journal.com

Hsp74/14-3-3σ Complex Mediates Centrosome Amplification by High Glucose, Insulin, and Palmitic Acid

Yu Cheng Lu, Pu Wang, Qi Gui Wu, Rui Kai Zhang, Alice Kong, Yuan Fei Li, and Shao Chin Lee**

It has been reported recently that type 2 diabetes promotes centrosome amplification via 14-3-3σ/ROCK1 complex. In the present study, 14-3-3σ interacting proteins are characterized and their roles in the centrosome amplification by high glucose, insulin, and palmitic acid are investigated. Co-immunoprecipitation in combination with MS analysis identified 134 proteins that interact with 14-3-3σ, which include heat shock 70 kDa protein 4 (Hsp74). Gene ontology analyses reveal that many of them are enriched in binding activity. Kyoto Encyclopedia of Genes and Genomes analysis shows that the top three enriched pathways are ribosome, carbon metabolism, and biosynthesis of amino acids. Molecular and functional investigations show that the high glucose, insulin, and palmitic acid increase the expression and binding of 14-3-3σ and Hsp74 as well as centrosome amplification, all of which are inhibited by knockdown of 14-3-3σ or Hsp74. Moreover, molecular docking analysis shows that the interaction between the 14-3-3σ and the Hsp74 is mainly through hydrophobic contacts and a lesser degree ionic interactions and hydrogen bond by different amino acids residues. In conclusion, the results suggest that the experimental treatment triggers centrosome amplification via upregulations of expression and binding of 14-3-3σ and Hsp74.

1. Introduction

Type 2 diabetes mellitus (T2DM) is a serious health problem worldwide, which can cause various chronic complications.[1] There is evidence that T2DM is associated with increased cancer risk and poor cancer prognosis. Currently, about 8–18% of all cancer patients have preexisting diabetes.[2] Individuals with diabetes who develop cancer have a 42% increased risk of death, a 21% increased risk of recurrence, and a significantly decreased 5-year overall and cancer-specific survival rate, as compared to individuals with cancer but free of diabetes.[3] However, little is known about the biological links between diabetes and cancer. It is speculated that deregulation of insulin and insulin-like growth factor signaling, obesity and inflammation, metabolic symbiosis, endoplasmic reticulum stress, and autophagy might play their roles.

Centrosome is the main microtubule organizing center. Each centrosome has two centrioles surrounded by the pericentriolar material, which plays important roles in cell division and the maintenance of genomic stability.[4] Centrosome amplification, acquisition of more than two centrosomes in each cell, is commonly found in various types of cancers, including solid tumors and hematological malignancies.[5] Recent experimental results suggest that centrosome amplification can initiate tumorigenesis[6] and increase cancer cell invasion potential.[7] Moreover, it is associated with poor cancer prognosis.[8]

T2DM presents typical pathophysiological features that include hyperglycemia, hyperinsulinemia, and increased level of free fatty acids. Palmitic acid, the most common saturated free fatty acid, is often used to investigate the effects of free fatty acids, in particular the adverse effects.[9] We have recently reported that T2DM promotes cell centrosome amplification via

Dr. Y. C. Lu, Dr. P. Wang, Q. G. Wu, R. K. Zhang, Prof. S. C. Lee
School of Life Sciences
Shanxi University
Taiyuan, Shanxi, 030006, P. R. China
Dr. Y. C. Lu
Central Laboratory
Linyi People's Hospital
Linyi, Shandong, 276000, P. R. China
Prof. A. Kong
Department of Medicine and Therapeutics
the Chinese University of Hong Kong
Shatin, Hong Kong SAR, 999077, P. R. China
Prof. Y. F. Li
Department of Oncology
First Clinical Hospital of Shanxi Medical University
Taiyuan, Shanxi, 030001, P. R. China
E-mail: liyflinda@163.com
Prof. S. C. Lee
School of Life Sciences
Jiangsu Normal University
Xuzhou, Jiangsu, 221010, P. R. China
E-mail: lee_shao@hotmail.com

DOI: 10.1002/pmic.201800197

AKT-ROS-dependent signaling of 14-3-3σ and ROCK1,[10] and the pathophysiological factors in T2DM are the triggers. These results implicate that centrosome amplification is a candidate biological link between T2DM and cancer development. In a functional proteomic study, we identified nine proteins associated with centrosome amplification, which included 14-3-3σ, NPM, and PCNA, which were all confirmed to mediate the centrosome amplification by high glucose, insulin, and palmitic acid.[11] The results emphasize that 14-3-3σ and its binding partners play important roles in the occurrence of the diabetes-associated centrosome amplification.

14-3-3 Proteins are a group of highly conserved, acidic proteins that have diverse intracellular functions, including intracellular signaling, cell division, apoptosis, cell cycle, and mitogenic signaling.[12] 14-3-3 Proteins are the key points in G1/S and G2/M transition.[13] The interaction between 14-3-3zeta and Polo-like kinase 1 ensures a faithful cytokinesis.[14] 14-3-3 Proteins of higher eukaryotes contribute to cell cycle regulation and/or centrosome-related functions by controlling protein binding dynamics at centrosomes.[15] In mammals, there are seven distinct isoforms of 14-3-3 (β, γ, ε, ζ, η, σ, and τ/θ).[16] 14-3-3γ Binds to γ-Tubulin, localizes to the centrosome, and can prevent centrosome amplification.[17]14-3-3σ is considered to be an important tumor suppressor and plays an important role in drug resistance.[18]

In this study, to better understand the mechanisms of how 14-3-3σ promotes the T2DM-associated centrosome amplification, we characterized the 14-3-3σ binding partners using co-immunoprecipitation (CoIP) followed by MS, and further investigated the roles of the binding partners of interest in the occurrence of the centrosome amplification trigged by high glucose, insulin, and palmitic acid.

Significance Statement

Type 2 diabetes increases the risk of all-site cancer, except prostate cancer. Centrosome amplification is sufficient to initiate tumorigenesis. We have recently reported that type 2 diabetes promotes centrosome amplification in vivo and protein 14-3-3σ is a signal mediator, which provides a candidate biological link between diabetes and cancer. However, the molecular mechanisms underlying the diabetes-associated centrosome amplification remain unknown. The present study has shown that 14-3-3σ interacts with various proteins through co-immunoprecipitation in combination with proteomic analysis, which occur concomitantly with the centrosome amplification. More specifically, 14-3-3σ interacts with Hsp74 mainly via hydrophobic contacts to form a complex that mediates the centrosome amplification. The results provide the directions for preventing the centrosome amplification and its adverse consequences in patients with type 2 diabetes by targeting at the Hsp74/14-3-3σ protein complex. The results also highlight the advantages of analyzing protein–protein interactions using proteomic analysis strategy.

2. Experimental Section

2.1. Chemicals, Antibodies, and Cell

All chemicals were purchased from Sigma (St. Louis, MO, USA). Anti-γ-tubulin antibody (no. ab27074; mouse antibody) was purchased from Abcam (Cambridge, UK). Anti-14-3-3σ antibody (no. PLA0201; rabbit antibody) was purchased from Sigma. Anti-heat shock protein 70 kDa protein 4 (Hsp74) antibody (no. ab137631; rabbit antibody) was provided by Abcam. Other antibodies were provided by Cell Signaling Technology (Boston, MA, USA).
HCT116 colon cancer cells were kindly provided by Dr. B. Vogelstein of the Johns Hopkins University School of Medicine. The culture medium and reagents were purchased from Gibco (Beijing, China). The palmitic acid stock was conjugated to fatty acid-free bovine albumin in a 3:1 molar ratio at 37 °C for 1 h before use. Anti-gamma tubulin antibody was used to detect centrosome by immunofluorescent staining.

2.2. Cell Culture and Experimental Treatment

HCT116 cells were maintained in the DMEM (glucose, 5 mM) supplemented with 10% fetal bovine serum, and 1% penicillin–streptomycin in a humidified incubator with 5% CO_2 at 37 °C. Cells from the cultures at ≈70% confluence were used for all experimental treatments. Cells treated for 48 h were used for quantification of centrosome number. Time course assays were performed and the time point was chosen, since this time point produced the significant level of differences for centrosome amplification between the control and the treated samples. Cells treated for 30 h were used for CoIP and Western blot analysis. The experimental treatment included high glucose (15 mM), insulin (150 nM), and palmitic acid (150 μM).

2.3. Confocal Microscopy

A cover slip was placed in a well of a six-well plate. Cells were plated at a density of 50 000 cells per well. Cells grown on the cover slips were fixed in cold methanol and acetone (1:1; v/v) for 6 min at –20 °C, followed by three washes with PBS (10 min each time). Then, the cells were incubated with 0.1% Triton X-100 for 15 min and 3% BSA for 1 h. The cells were incubated with a primary antibody in 3% BSA in PBS overnight at 4 °C, washed twice with PBS, and incubated with an FITC-conjugated secondary antibody in 3% BSA in PBS for 1 h at room temperature in the dark. Finally, the cells were mounted with mounting medium. Confocal microscopy was performed using the Zeiss LSM880 microscope (Oberkochen, Germany) with a 1.4 NA oil-immersion lens, and image processing was performed with Zen software (Oberkochen, Germany).

2.4. CoIP Assay

The HCT116 cells were seeded in 10 cm dishes at a cell number of 5×10^6. After treatment, cells were harvested and lysed in 500 μL precooled CoIP buffer (50 mM Tris/HCl pH 8.0, 150 mM NaCl, 5 mM EDTA, 0.5% NP-40, 1 mM phenylmethylsulfonyl fluoride, 2 μg mL^{-1} leupeptin, and 2 μg mL^{-1} pepstatin A) for

30 min on ice. After centrifugation (14 000 rpm, 4 °C, 15 min), the supernatants were mixed with 30 μL protein A agarose bead slurry and incubated with rotation at 4 °C for 1 h. Following by centrifugation (14 000 rpm, 4 °C, 15 min), the supernatants were incubated with the primary antibody at 4 °C overnight. The next day, mixture was mixed with 10–30 μL bead slurry for 3 h at 4 °C. After three times of washing with CoIP buffer in 50 μL elution buffer with shaking (100 mM Gly-Cl pH 2.5, 500 mM NaCl, 0.05% Tween-20) for 1 min. After centrifugation (3000 rpm, 4 °C, 3 min), the supernatants were collected and 250 μL neutralization buffer (1 M Tris-Cl pH 8.0) were added. The samples were used for quantification of protein concentration then MS analysis.

2.5. Filter-Aided Sample Preparation

The eluted proteins were then digested according to the filter-aided sample preparation (FASP) procedure described. Briefly, 200 μg of proteins for each sample (supernatant) were incorporated into 30 μL SDT buffer (4% SDS, 100 mM DTT, 150 mM Tris-HCl pH 8.0) at 90 °C for 5 min. The detergent DTT and other low-molecular-weight components were removed using 200 μL UA buffer (8 M urea, 150 mM Tris-HCl pH 8.0) by repeated ultrafiltration (Microcon units, 30 kDa). Then 100 μL 0.05 M iodoacetamide in UA buffer was added to block reduced cysteine residues and the samples were incubated for 20 min in darkness. The filter was washed with 100 μL UA buffer three times and then twice with 100 μL 25 mM NH_4HCO_3. Finally, the protein suspension was digested with 2 μg trypsin (Promega) in 40 μL 25 mM NH_4HCO_3 overnight at 37 °C, and the resulting peptides were collected as a filtrate.

2.6. LC–ESI–MS/MS Analysis by Q Exactive

Experiments were performed on a Q Exactive mass spectrometer that was coupled to Easy nLC (Proxeon Biosystems, now Thermo Fisher Scientific). Six microliters of each fraction was injected for nanoLC–MS/MS analysis. The peptide mixture (5 μg) was loaded onto a the C18-reversed phase column (Thermo Scientific Easy Column, 10 cm long, 75 μm inner diameter, 3μm resin) in buffer A (0.1% formic acid) and separated with a linear gradient of buffer B (80% acetonitrile and 0.1% formic acid) at a flow rate of 250 nL min^{-1} controlled by IntelliFlow technology over 140 min. MS data were acquired using a data-dependent top 10 method dynamically choosing the most abundant precursor ions from the survey scan (300–1800 m/z) for high-energy collision-induced dissociation fragmentation. Determination of the target value is based on predictive automatic gain control. Dynamic exclusion duration was 60 s. Survey scans were acquired at a resolution of 70 000 at m/z 200 and resolution for HCD spectra was set to 17 500 at m/z 200. Normalized collision energy was 30 eV and the underfill ratio, which specifies the minimum percentage of the target value likely to be reached at maximum fill time, was defined as 0.1%. The instrument was run with peptide recognition mode enabled.

2.7. Sequence Database Searching and Data Analysis

All MS/MS spectra were searched using Mascot software v2.2.2 software (Matrix Science, London, UK), against the *Homo sapiens* UniProtKB database (www.uniprot.org). For protein identification, the following options were used: Peptide mass tolerance, 20 ppm; MS/MS tolerance, 0.1 Da; enzyme, trypsin; and missed cleavage, 2. Fixed modification was carbamidomethyl. Variable modification: oxidation.

2.8. Bioinformatic Analysis

To examine the biological and functional properties of the identified proteins, Gene ontology (GO) annotation was conducted by searching the GO database (http://www.geneontology.org). Functional category analysis was performed with protein2go and go2protein for annotation. Visualization and Integrated Discovery v6.7 was used for functional enrichment analysis of GO terms and KEGG pathways. A false discovery rate of <0.01 was selected as the cut-off criterion.

2.9. Small Interfering RNA and Transfection

For the siRNA studies, the pre-designed small interfering RNA (siRNA) oligonucleotides (Sangon Technology, Shanghai, China) were: 1) 14-3-3σ, ACCUGCUCUCAGUAGCCUATT (sense) and UAGGCUACUGAGAGCAGGUTT (anti-sense) and 2) Hsp74, AGGACGAGUUUGAG CACAATT (sense) and UUGUGCUCAAACUCGUCCUTT (anti-sense). HCT116 cells (5×10^4 cells per well) were seeded in six-well plates and cultured for 24 h, and then were transfected with 200 pM siRNA oligonucleotides using Lipofectamine 2000 transfection reagent (Invitrogen, California, USA), according to the manufacturer's instructions. The protein level was evaluated by Western blot analysis.

2.10. Western Blot Analysis

The cells were lysed in RIPA buffer. Proteins were separated by PAGE and transferred onto polyvinylidene fluoride membrane. After blocking for 1 h at room temperature with TBST containing 0.05% (v/v) Tween-20 and 5% (w/v) non-fat milk, the membranes were incubated with primary antibodies overnight at 4 °C, followed by washes with TBST containing 0.05% Tween-20. The membranes were then incubated with a horseradish peroxidase-conjugated secondary antibody for 1 h at room temperature. ECL reagents (Thermo Biosciences, Massachusetts, USA) were used to visualize the protein bands which were captured on X-ray film.

2.11. Homology Modeling and Molecular Docking

To further elucidate the functional relationships between 14-3-3σ and interacting proteins, a protein of interests was chosen, which is Hsp74. The crystallographic structure of the Hsp74 has not been published yet. In order to expose the binding mode between human 14-3-3σ protein and Hsp74 at the molecular level, the 3D structure of the Hsp74 was

built by means of modeler 9.19 homology modeling software (http://salilab.org/modeller/). The sequence in FASTA format of Hsp74 was retrieved from NCBI (Accession: P34932.4). The crystallographic structure of *Saccharomyces cerevisiae* Hsp110 (PDB ID: 3C7N) was selected as the templates for modeling. Molecular docking were performed to investigate the binding mode between the human 14-3-3σ protein and the Hsp74 using the ZDOCK server (http://zdock.umassmed.edu/). The 3D structure of the human 14-3-3σ (PDB ID: 6FCP) was downloaded from Protein Data Bank (http://www.rcsb.org/pdb/home/home.do), while the 3D structure of the Hsp74 was built by modeler 9.19. For docking, the default parameters were used as described in the ZDOCK server. The top ranked pose as judged by the docking score was using PyMoL 1.7.6 software (http://www.pymol.org/).

2.12. Statistical Analysis

All the experiments were performed in triplicate. Data were expressed as the mean ± SD. Student's *t*-test was performed for comparison between two groups. The statistical analysis software package SPSS 21.0 was employed for the statistical comparisons. A p-value < 0.05 was considered significant.

3. Results

3.1. High Glucose, Insulin, and Palmitic Acid Induce Centrosome Amplification

We have recently reported that the level of centrosome amplification is increased in peripheral blood mononuclear cells from patients with type 2 diabetes. AKT-ROS-dependent upregulation of 14-3-3σ and ROCk1 as well as their binding and translocation to centrosome is the underlying signal transduction pathway for the diabetes-associated centrosome amplification.[10] In the present study, we further investigated the molecular basis of centrosome amplification associated with T2DM using colon cancer cells as an experimental model, which were treated with high glucose, insulin, and palmitic acid. As shown in **Figure 1**A,B, high glucose, insulin, and palmitic acid were able to induce moderate centrosome amplification in the cells. Under the experimental conditions, most cells with centrosome amplification had three to five centrosomes per cell (Figure 1A). Glucose, insulin, and palmitic acid were used at 15 mM, 5 nM, and 150 μM, respectively, which were close to their pathophysiological levels.

3.2. Identification of 14-3-3σ-Interacting Proteins

To characterize proteins attached to the 14-3-3σ, we performed CoIP using 14-3-3σ antibody and identified the partner proteins using MS. As shown in **Table 1**, a total of 165 proteins were identified, among which 134 protein were identified from the treated samples, 19 proteins were identified from the control samples and 12 proteins were identified from both control and treated samples (**Figure 2**). Thus, 153 proteins were responsive to the experimental treatment.

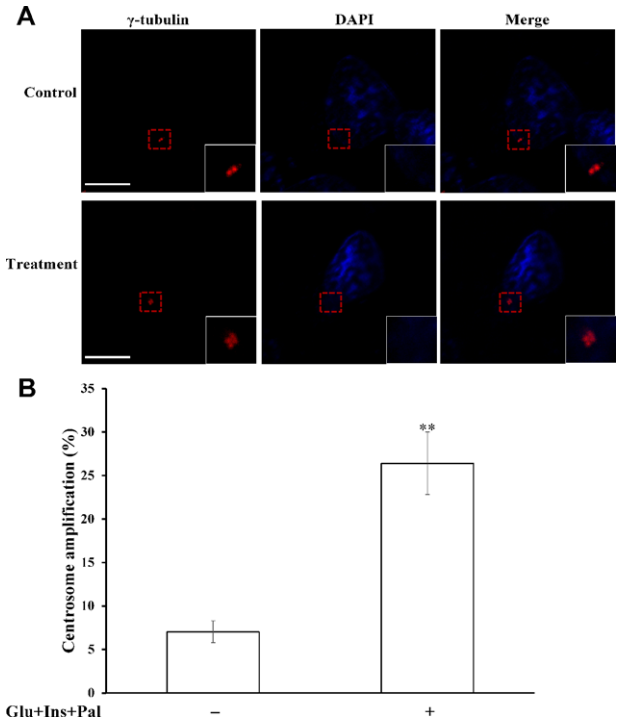

Figure 1. High glucose, insulin, and palmitic acid induce centrosome amplification. A) Images of centrosome and centrosome amplification; B) high glucose, insulin, and palmitic acid increased centrosome amplification in HCT 116 cells. Glu: glucose, 15 mM; Ins: insulin, 5 nM; Pal: palmitic acid, 150 μM. $^{**}p < 0.01$, compared with that in the control group. White scale bar represents 5 μm.

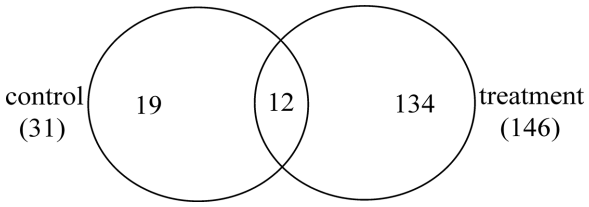

Figure 2. Venn diagram shows the numbers of identified proteins from the control and treated HCT 116 cells. Each number with no overlap of circles showed the number of proteins uniquely observed in that sample, while the overlapping circle showed the numbers of identified proteins common to two of the analyzes.

3.3. Bioinformatics Analysis of the 14-3-3σ Binding Proteins

GO clustering analysis was performed to provide relevant information about their biological processes, molecular functions, and cellular components. Totally, there were 134 14-3-3σ interacting proteins. One-hundred thirty-one (97.76%) proteins were categorized into biological process, 133 (99.25%) proteins were involved in molecular functions, and 133 (99.25%) proteins were grouped into cellular components. Within the biological processes category, the majority of the proteins were involved in cellular process and metabolic process. For molecular functions, the data indicated that most of the proteins were linked to binding, catalytic activity, and structural molecule activity. Regarding cellular components, cell, organelle, and cell part were the top-ranked

Table 1. Identification of 14-3-3σ-interacting proteins in control and treated samples using MS.

Source of proteins	Uniprot ID	Protein name	Theoretical MW [KDa]	Number of peptides	Number of unique petides	Cover percent [%]
Proteins from treated samples	P09429	High mobility group protein B1	24.893	2	2	11.6
	E9PAV3	Nascent polypeptide-associated complex subunit alpha, muscle-specific form	205.42	1	1	0.6
	B4DX78	cDNA FLJ55484, highly similar to ATP-dependent RNA helicase DDX39 (EC 3.6.1.-)	53.696	1	1	2.6
	O00299	Chloride intracellular channel protein 1	26.922	1	1	3.7
	Q93008	Probable ubiquitin carboxyl-terminal hydrolase FAF-X	292.28	1	1	0.7
	Q8TAA3	Proteasome subunit alpha type-7-like	28.529	1	1	4.3
	O15143	Actin-related protein 2/3 complex subunit 1B	40.949	1	1	3.5
	O43175	D-3-Phosphoglycerate dehydrogenase	56.65	1	1	2.1
	O75368	SH3 domain-binding glutamic acid-rich-like protein	12.774	1	1	11.4
	O75390	Citrate synthase, mitochondrial	51.712	1	1	3.4
	O95433	Activator of 90 kDa heat shock protein ATPase homolog 1	38.274	1	1	3.6
	P00505	Aspartate aminotransferase, mitochondrial	47.517	1	1	3.3
	P00558	Phosphoglycerate kinase 1	44.614	4	4	9.6
	P02545	Prelamin-A/C	74.139	4	3	6.2
	P04406	Glyceraldehyde-3-phosphate dehydrogenase	36.053	1	1	8.7
	P05388	60S acidic ribosomal protein P0	34.273	1	1	8.8
	P06454	Prothymosin alpha	12.203	3	3	22.5
Proteins from treated samples	P06576	ATP synthase subunit beta, mitochondrial	56.559	2	2	4.9
	P06733	Alpha-enolase	47.168	3	3	14.1
	P06748	Nucleophosmin	32.575	1	1	10.9
	B4DY90	Tubulin beta chain	52.048	3	2	8
	P07737	Profilin-1	15.054	2	1	24.3
	P07900	Heat shock protein HSP 90-alpha	84.659	4	2	12.3
	P08238	Heat shock protein HSP 90-beta	83.263	9	6	19.6
	P08758	Annexin A5	35.936	2	2	6.2
	A0A0C4DG17	40S ribosomal protein SA	33.313	2	2	10
	P09382	Galectin-1	14.716	1	1	8.9
	P09651	Heterogeneous nuclear ribonucleoprotein A1	38.746	1	1	12.4
	P0DME0	Protein SETSIP	34.882	1	1	3.3
	P16402	Histone H1.3	22.35	1	1	5
	P11021	78 kDa Glucose-regulated protein	72.332	4	4	12.7
	P13639	Elongation factor 2	95.337	2	2	3.8
	P13667	Protein disulfide-isomerase A4	72.932	1	1	2.2
	P13796	Plastin-2	70.288	3	3	5.7
	P13929	Beta-enolase	46.986	1	1	3.2
	P14174	Macrophage migration inhibitory factor	12.476	1	1	9.6

(*Continued*)

Table 1. Continued.

Source of proteins	Uniprot ID	Protein name	Theoretical MW [KDa]	Number of peptides	Number of unique petides	Cover percent [%]
	P14625	Endoplasmin	92.468	4	3	5.5
	B4E1U9	cDNA FLJ54776, highly similar to Cell division control protein 42 homolog	26.528	1	1	4.7
	J7M2B1	Tyrosine-protein kinase receptor	98.947	1	1	1.2
Proteins from treated samples	P15531	Nucleoside diphosphate kinase A	17.149	3	3	23
	P17844	Probable ATP-dependent RNA helicase DDX5	69.147	1	1	1.5
	P17987	T-complex protein 1 subunit alpha	60.343	2	2	8.1
	P18669	Phosphoglycerate mutase 1	28.804	1	1	10.2
	P19338	Nucleolin	76.613	1	1	5.1
	B3KXY9	cDNA FLJ46359 fis, clone TESTI4049786, highly similar to Hexokinase-1 (EC 2.7.1.1)	106.25	1	1	1.2
	P20700	Lamin-B1	66.408	2	1	3.6
	P22087	rRNA 2-O-methyltransferase fibrillarin	33.784	1	1	4
	P22626	Heterogeneous nuclear ribonucleoproteins A2/B1	37.429	3	3	10.5
	P23246	Splicing factor, proline- and glutamine-rich	76.149	1	1	1.6
	P23396	40S ribosomal protein S3	26.688	2	2	7.4
	P23526	Adenosylhomocysteinase	47.716	1	1	2.8
	E9PK25	Cofilin-1	22.728	3	3	15.7
	B4DRM3	cDNA FLJ54492, highly similar to Eukaryotic translation initiation factor 4B	69.725	1	1	1.8
	P25398	40S ribosomal protein S12	14.515	1	1	7.6
	P25705	ATP synthase subunit alpha, mitochondrial	59.75	1	1	6.3
	P25788	Proteasome subunit alpha type-3	28.433	1	1	3.9
	P26641	Elongation factor 1-gamma	50.118	2	2	5.3
	P27348	14-3-3 protein theta	27.764	1	1	5.7
	P27797	Calreticulin	48.141	2	2	4.8
	Q53XS4	Tyrosine-protein phosphatase non-receptor type	67.718	1	1	1.5
Proteins from treated samples	P29401	Transketolase	67.877	1	1	1.4
	P29692	Elongation factor 1-delta	31.121	1	1	3.2
	P30041	Peroxiredoxin-6	25.035	1	1	5.4
	P30086	Phosphatidylethanolamine-binding protein 1	21.057	1	1	7.5
	P30101	Protein disulfide-isomerase A3	56.782	3	3	6.3
	P34932	Heat shock 70 kDa protein 4	94.33	2	1	3
	P35268	60S ribosomal protein L22	14.787	1	1	10.2
	Q13344	Fus-like protein (Fragment)	53.376	1	1	7.8
	P36578	60S ribosomal protein L4	47.697	1	1	4.4
	P37837	Transaldolase	37.54	1	1	3.9
	P39023	60S ribosomal protein L3	46.108	1	1	3
	P40227	T-complex protein 1 subunit zeta	58.024	1	1	2.1

(*Continued*)

Table 1. Continued.

Source of proteins	Uniprot ID	Protein name	Theoretical MW [KDa]	Number of peptides	Number of unique petides	Cover percent [%]
	P40926	Malate dehydrogenase, mitochondrial	35.503	2	2	7.4
	F6WQW2	Ran-specific GTPase-activating protein	31.904	2	2	7.2
	Q59GX9	Ribosomal protein L5 variant (Fragment)	35.203	1	1	3
	P50990	T-complex protein 1 subunit theta	59.62	2	2	4
	P50991	T-complex protein 1 subunit delta	57.924	1	1	7.2
	P50993	Sodium/potassium-transporting ATPase subunit alpha-2	112.26	1	1	1.2
	P52597	Heterogeneous nuclear ribonucleoprotein F	45.671	1	1	6.5
	P55072	Transitional endoplasmic reticulum ATPase	89.321	2	2	2.2
	F8VVS7	Caspase	46.452	1	1	2.4
	P57721	Poly(rC)-binding protein 3	39.465	1	1	3
Proteins from treated samples	P60174	Triosephosphate isomerase	30.791	1	1	4.5
	B7Z6Z4	Myosin light polypeptide 6	26.707	1	1	3.4
	P60842	Eukaryotic initiation factor 4A-I	46.153	5	5	14.8
	P61158	Actin-related protein 3	47.371	1	1	2.9
	P61160	Actin-related protein 2	44.76	1	1	3
	P61247	40S ribosomal protein S3a	29.945	1	1	11.4
	P61313	60S ribosomal protein L15	24.146	1	1	4.4
	K7ELC7	60S ribosomal protein L27 (Fragment)	16.359	2	2	13.2
	Q5EC54	Heterogeneous nuclear ribonucleoprotein K transcript variant	51.058	3	3	7.1
	P61981	14-3-3 protein gamma	28.302	1	1	4.5
	P62241	40S ribosomal protein S8	24.205	1	1	3.4
	Q6IPX4	40S ribosomal protein S16	17.107	1	1	6.6
	G9K388	YWHAE/FAM22A fusion protein (Fragment)	41.224	1	1	2.9
	P62269	40S ribosomal protein S18	17.718	1	1	7.2
	P62277	40S ribosomal protein S13	17.222	2	2	12.6
	P62280	40S ribosomal protein S11	18.431	1	1	7
	P62701	40S ribosomal protein S4, X isoform	29.597	2	2	8.4
	J3KQE5	GTP-binding nuclear protein Ran (Fragment)	26.816	1	1	3.8
	P62906	60S ribosomal protein L10a	24.831	1	1	6
	A0A087WZM5	Peptidylprolyl isomerase	14.926	1	1	10.1
	I3L504	Eukaryotic translation initiation factor 5A-1	20.503	1	1	18.8
	P63244	Receptor of activated protein C kinase 1	35.076	3	3	10.4
Proteins from treated samples	P63261	Actin, cytoplasmic 2	41.792	14	1	48.3
	P68371	Tubulin beta-4B chain	49.83	3	2	8.8
	K7ES00	Histone H3.3 (Fragment)	16.621	2	2	10.6

(*Continued*)

Table 1. Continued.

Source of proteins	Uniprot ID	Protein name	Theoretical MW [KDa]	Number of peptides	Number of unique petides	Cover percent [%]
	P84103	Serine/arginine-rich splicing factor 3	19.329	1	1	5.5
	A0A087WVQ6	Clathrin heavy chain	192.06	1	1	0.7
	Q00839	Heterogeneous nuclear ribonucleoprotein U	90.583	1	1	1
	Q01130	Serine/arginine-rich splicing factor 2	25.476	1	1	7.7
	Q01518	Adenylyl cyclase-associated protein 1	51.901	1	1	1.5
	Q02543	60S ribosomal protein L18a	20.762	1	1	7.4
	Q02790	Peptidyl-prolyl cis-trans isomerase FKBP4	51.804	1	1	2.8
	Q9HBB3	60S ribosomal protein L6	32.891	1	1	3.1
	Q04917	14-3-3 Protein eta	28.218	1	1	4.1
	Q0P6D2	Protein FAM69C	46.42	1	1	3.6
	Q13162	Peroxiredoxin-4	30.54	2	1	7
	Q14103	Heterogeneous nuclear ribonucleoprotein D0	38.434	1	1	2.8
	Q15084	Protein disulfide-isomerase A6	48.121	2	2	6.4
	Q8IYT4	Katanin p60 ATPase-containing subunit A-like 2	61.252	1	1	2.2
	B4DFR2	cDNA FLJ59194, moderately similar to Dynein light chain 2A, cytoplasmic	13.362	1	1	7.4
	Q93045	Stathmin-2	20.828	1	1	5.6
	Q9BT56	Spexin	13.302	1	1	7.8
	Q9BTT0	Acidic leucine-rich nuclear phosphoprotein 32 family member E	30.692	1	1	10.8
Proteins from treated samples	Q9P258	Protein RCC2	56.084	1	1	3.3
	Q9UHV9	Prefoldin subunit 2	16.648	1	1	9.1
	A0A0S2Z4G4	Tropomyosin 3 isoform 1 (Fragment)	29.032	2	2	6
	A0A0G2JJA7	Proteasome subunit beta type	20.941	1	1	8.2
	B4DDB6	Heterogeneous nuclear ribonucleoprotein A3, isoform CRA_a	37.029	2	2	6.5
	D6RDG3	Transcription factor BTF3 (Fragment)	11.802	1	1	11.9
	Q71V99	Peptidyl-prolyl cis-trans isomerase	17.971	4	1	28.7
	Q9BZT5	PNAS-26	13.934	1	1	13
	B2KLP9	NADH-ubiquinone oxidoreductase chain 1	35.662	1	1	7.9
Proteins from control samples	A6NKL6	Transmembrane protein 200C	63.927	1	1	1.3
	A0A075B6H0	Receptor-type tyrosine-protein phosphatase T	163.97	1	1	1.6
	O75170	Serine/threonine-protein phosphatase 6 regulatory subunit 2	104.94	1	1	0.7
	P06702	Protein S100-A9	13.242	1	1	11.4

(*Continued*)

Table 1. Continued.

Source of proteins	Uniprot ID	Protein name	Theoretical MW [KDa]	Number of peptides	Number of unique petides	Cover percent [%]
	P15924	Desmoplakin	331.77	3	3	1.4
	P17066	Heat shock 70 kDa protein 6	71.027	1	1	4.5
	P29508	Serpin B3	44.564	1	1	2.6
	P32969	60S ribosomal protein L9	21.863	1	1	14.1
	Q8N1C8	HSPA9 protein (Fragment)	73.853	2	2	7.5
	Q01469	Fatty acid-binding protein, epidermal	15.164	1	1	13.3
	F4ZW66	NF110b	95.777	1	1	1.3
	Q5T749	Keratinocyte proline-rich protein	64.135	2	2	4.7
Proteins from control samples	Q8N4B1	Sesquipedalian-1	27.215	1	1	4
	Q8WTW4	Nitrogen permease regulator 2-like protein	43.658	1	1	3.4
	Q9H165	B-cell lymphoma/leukemia 11A	91.196	1	1	1.9
	Q9HCR9	Dual 3,5-cyclic-AMP and -GMP phosphodiesterase 11A	104.75	1	1	2.6
	B4DZQ0	cDNA FLJ59289, highly similar to Retinoblastoma-binding protein 6 (Fragment)	113.46	1	1	1.7
	H7C2W5	NADH dehydrogenase [ubiquinone] 1 alpha subcomplex subunit 10, mitochondrial (Fragment)	15.09	1	1	6.2
	Q5T6K5	Nuclear transcription factor Y subunit gamma (Fragment)	34.212	1	1	3.5
Common proteins from the control sample and treated sample	B4DR52	Histone H2B	18.041	2	2	24.7
	J3KPS3	Fructose-bisphosphate aldolase	39.817	1	1	10.9
	P04908	Histone H2A type 1-B/E	14.135	1	1	15.4
	P10599	Thioredoxin	11.737	1	1	8.6
	P10809	60 kDa Heat shock protein, mitochondrial	61.054	1	1	12.7
	P11142	Heat shock cognate 71 kDa protein	70.897	3	3	23.5
	P14618	Pyruvate kinase PKM	57.936	1	1	17.3
	H0Y7A7	Calmodulin (Fragment)	20.762	1	1	15.5
	P62805	Histone H4	11.367	2	2	31.1
	P68104	Elongation factor 1-alpha 1	50.14	2	2	10.2
	Q06830	Peroxiredoxin-1	22.11	1	1	32.2
	Q96SB8	Structural maintenance of chromosomes protein 6	126.32	1	1	0.6

categories (**Figure 3**A–C). KEGG pathway enrichment analysis revealed that the 14-3-3σ-interacting proteins were related to 149 pathways. The 20 highly enriched pathways are shown in Figure 3D. The five most significantly enriched were ribosome, carbon metabolism, biosynthesis of amino acids, PI3K–AKT signaling pathway, and protein processing in ER.

3.4. Hsp74 Mediates the Centrosome Amplification

From the proteins pulled down using 14-3-3σ antibody, we were interested in Hsp74. Why we targeted at Hsp74? The protein came to our attention, as several Hsp proteins are present in centrosome,[19] which suggests that Hsp proteins may play roles in centrosome homeostasis. Moreover, Hsp proteins are known binding partners of 14-3-3 proteins.[20] Thus, we investigated whether Hsp74 contributed to the centrosome amplification. Indeed, we found that the expression level of Hsp74 was increased by high glucose, insulin, and palmitic acid, which was inhibited by Hsp74 specific siRNA (**Figure 4**A). Knockdown of Hsp74 using their siRNA downregulated the treatment-induced centrosome amplification (Figure 4B).

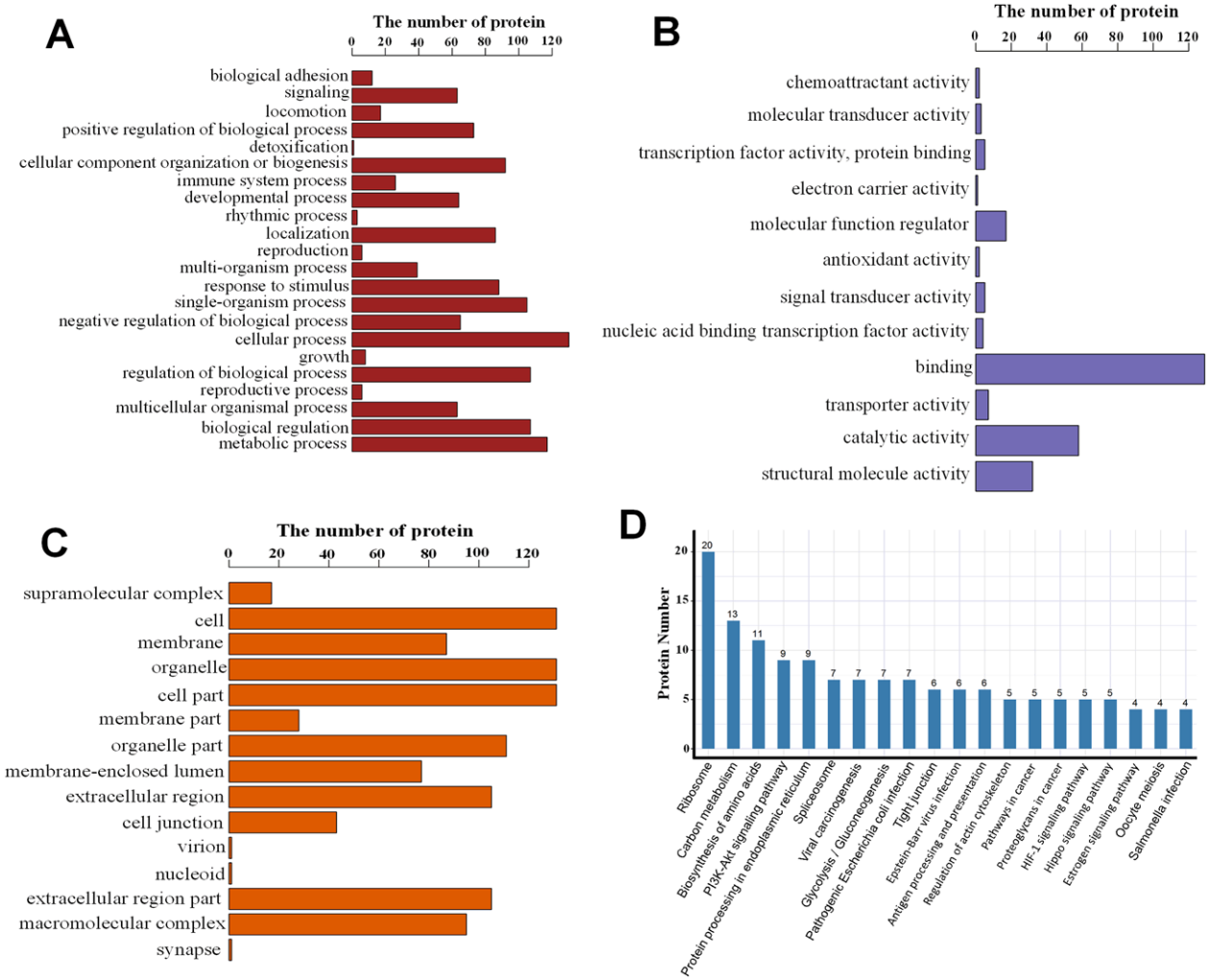

Figure 3. The results of bioinformatics analysis. GO categories of the 14-3-3σ-interacting differentially expression proteins. The identified proteins were classified into biological process (A), molecular function (B), and cellular component (C) by WEGO according to the GO terms. D) KEGG pathway analysis of the 14-3-3σ-interacting proteins. The top 20 enriched pathways are selected.

3. 5 14-3-3σ-Hsp74 Complex is Required for the Centrosome Amplification

We next performed experiments to confirm the binding between 14-3-3σ and Hsp74, and to examine whether 14-3-3σ and Hsp74 complex was required for the centrosome amplification. As expected, Hsp74 was pulled down by 14-3-3σ antibody (**Figure 5**A). Importantly, the binding between Hsp74 and 14-3-3σ was increased by high glucose, insulin, and palmitic acid (Figure 5A). If the Hsp74 /14-3-3σ complex mediated the treatment-induced centrosome amplification, inhibition or disruption of the complex would inhibit the centrosome amplification. siRNA technology was used to inhibit or disrupt the protein complex via protein knockdown of Hsp74 or 14-3-3σ. Indeed, individual knockdown of Hsp74 or 14-3-3σ protein level (Figure 5B) attenuated the treatment-induced centrosome amplification (Figures 4A,B and 5C). In addition, when Hsp74 was knocked down using siRNA, although Hsp74 was pulled down by 14-3-3σ antibody, the level was very low (Figure 5D). These data proved that the complex was reduced using siRNA of Hsp74.

3.6. Molecular Docking between 14-3-3σ and Hsp74

The interaction between the 14-3-3σ (green) and the Hsp74 (rose red) is shown in **Figure 6**A. Detailed analysis (Figure 6B) showed that one hydrophobic interaction was observed between the residues Leu-174, Val-178, Leu-218, Leu-222, Leu-223, and Leu-229 of the 14-3-3σ and the residues Phe-440, Tyr-445, and Tyr-446 of the Hsp74. Another hydrophobic interaction was observed between the residues Tyr-19, Val-51, Gly-54, Ala-57, Ala-58, Val-61, and Val-88 of the 14-3-3σ and the residues Leu-452, Pro-453, Tyr-454, Pro-457, Ala-458, Ile-459, Ala-460, and Phe-462 of the Hsp74, forming a strong hydrophobic binding. In addition, the residue Asp-225 of the 14-3-3σ formed anion–π interactions with the side chain of the residues Phe-440 and Tyr-446 of

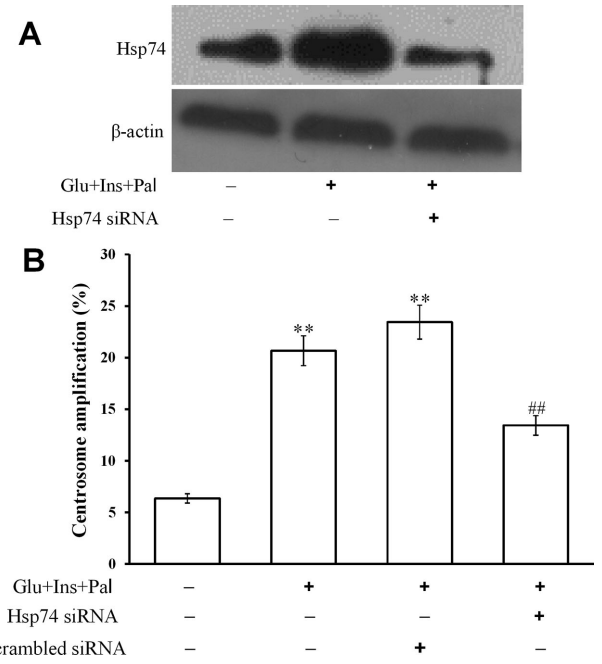

Figure 4. Hsp74 mediates the centrosome amplification. A) High glucose, insulin, and palmitic acid increased the protein level of Hsp74, which was inhibited by Hsp74 specific siRNA; B) knockdown of Hsp74 downregulated the centrosome amplification. Glu: glucose, 15 mM; Ins: insulin, 5 nM; Pal: palmitic acid, 150 μM. $^{**}p < 0.01$, compared with that in the control group; $^{\#\#}p < 0.01$, compared with that in the treatment group with siRNA.

the Hsp74. Moreover, the anion–π interaction was observed between the residue Glu-182 of the 14-3-3σ and the side chain of the residue Tyr-445 of the Hsp74. The residues Arg-56 and Arg-60 of the 14-3-3σ formed cation–π interactions with the residue Tyr-445 of the Hsp74. Importantly, six hydrogen bond interactions were shown between the residue Glu-182 of the 14-3-3σ and the Tyr-445 of the Hsp74 (bond length: 2.3 Å), the residue Asp-225 of the 14-3-3σ and the Ser-447 of the Hsp74 (bond length: 2.9 Å), the residue Arg-60 of the 14-3-3σ and the Asp-451 of the Hsp74 (bond length: 3.5 Å), the residue Tyr-19 of the 14-3-3σ and the Asp-456 of the Hsp74 (bond length: 3.5 Å), the residue Val-88 of the 14-3-3σ and the Gln-461 of the Hsp74 (bond length: 3.5 Å), and the Arg-18 of the 14-3-3σ and the Glu-499 of the Hsp74 (bond length: 3.4 Å). These were the main binding affinity between the 14-3-3σ and Hsp74.

4. Discussion

In the present study, we showed that high glucose, insulin, and palmitic acid could induce centrosome amplification (Figure 1A,B) and 14-3-3σ was a signal mediator, which is in agreement with our previous report that the experimental treatment induces centrosome amplification via ROCK1/14-3-3σ complex.[10] Moreover, previous report indicated 14-3-3 proteins interacted with over 200 human phosphoproteins in HeLa cells using 14-3-3 affinity chromatography.[21] Here, we identified 31 and 146 14-3-3σ binding proteins in the untreated and treated HCT116 cells, respectively, which included Hsp74 (Table 1, Figure 2). Compared with previous study, the reasons for the difference in the amount of interacted protein were: 1) different cell types and 2) different antibody used. Compared with untreated cells, the amount of treated cells proteins almost increased fivefold. The experimental treatment increased the abundance to several proteins in the centrosomes, which may be due to the treatment-promoted translocation of these proteins to the centrosomes, the role of which in the centrosome amplification require further examinations (Lu et al., unpublished data; Figure 5B).

Hsp74, also called Apg-2 (ATP and peptide-binding protein in germ cells-2),[22] is a member of the Hsp110 family. It was first described as Hsp70 RY from B cells[23] and is encoded by HSPA4 gene.[24] Hsp74 is inducible under various conditions, including cancer,[25] chronic inflammation,[26] and acidic pH stress.[27] It is overexpressed in various cancer cells and intestinal cells. Chen and co-workers reported that Hsp74 was highly expressed in bladder cancer and distributed into cytoplasm, which was associated with keratin 1.[28] Hsp74 also upregulates Bcl-2 and IL-17 in the gut, which controls cell apoptosis as well as immune response.[26] In addition, the synthesis of Hsp74 affects microtubules stability, which is related to cytoskeletal stability.[29] Centrosome comprises of a pair of centrioles surrounded by the pericentriolar material.[4] Centrioles comprise nine triplet microtubules, which are arranged into a cylinder with a diameter of ≈250 nm.[30] Whether Hsp74 modifies the stability of centriole for centrosome amplification remains unknown. In the present study, we showed that the overexpression of Hsp74 mediated centrosome amplification (Figure 4A,B). Furthermore, Hsp74 and 14-3-3σ formed a complex to promote centrosome amplification (Figure 5A–D) triggered by the experimental treatment, as disruption of the complex attenuated the treatment-elicited centrosome amplification.

14-3-3 Proteins, consisting of nine antiparallel α-helices forming a horseshoe-shaped dimer, play important roles in signal transduction pathways that control cell cycle checkpoints, MAP kinase activation, apoptosis, and gene expression.[31] In previous studies, 14-3-3 proteins recognize phosphorylated peptides in their binding partners. Muslin and colleagues showed that the optimal phosphopeptide motifs selected by different 14-3-3 isotypes are extremely similar, which is RSXpSXP.[32] Later, Yaffe et al. have reported that all 14-3-3 isotypes bind to common phosphoserine/phosphothreonine-containing peptide motifs corresponding to Mode-I (R(S/X)XpSXP) and Mode-II (RXXXpSXP or RXY/FXpSXP) sequences.[33] More recently, Ganguly et al. reported the third consensus binding motif (Mode-III, pS/pT-$X_{1\text{-}2}$-COOH).[34] The binding of the consensus motif I–III to 14-3-3 is regulated by the basic cluster of 14-3-3 residues consisting of Lys49, Arg56, and Arg127.[31]

In addition, 14-3-3 proteins also interact in a phosphorylation-independent manner with some target proteins, such as carbohydrate response element-binding protein (ChREBP),[35] exoenzyme S (ExoS),[36] human telomerase,[37] and the amyloid β-protein precursor intracellular domain fragment.[38] In 14-3-3-ChREBP interaction, the binding sequence of ChREBP was ^{121}RLNNAIWRAWY^{131} (the underlined residues are those in contact with 14-3-3). These binding sequences of ChREBP bind to 14-3-3 through a free sulfate/phosphate molecule. Moreover, several

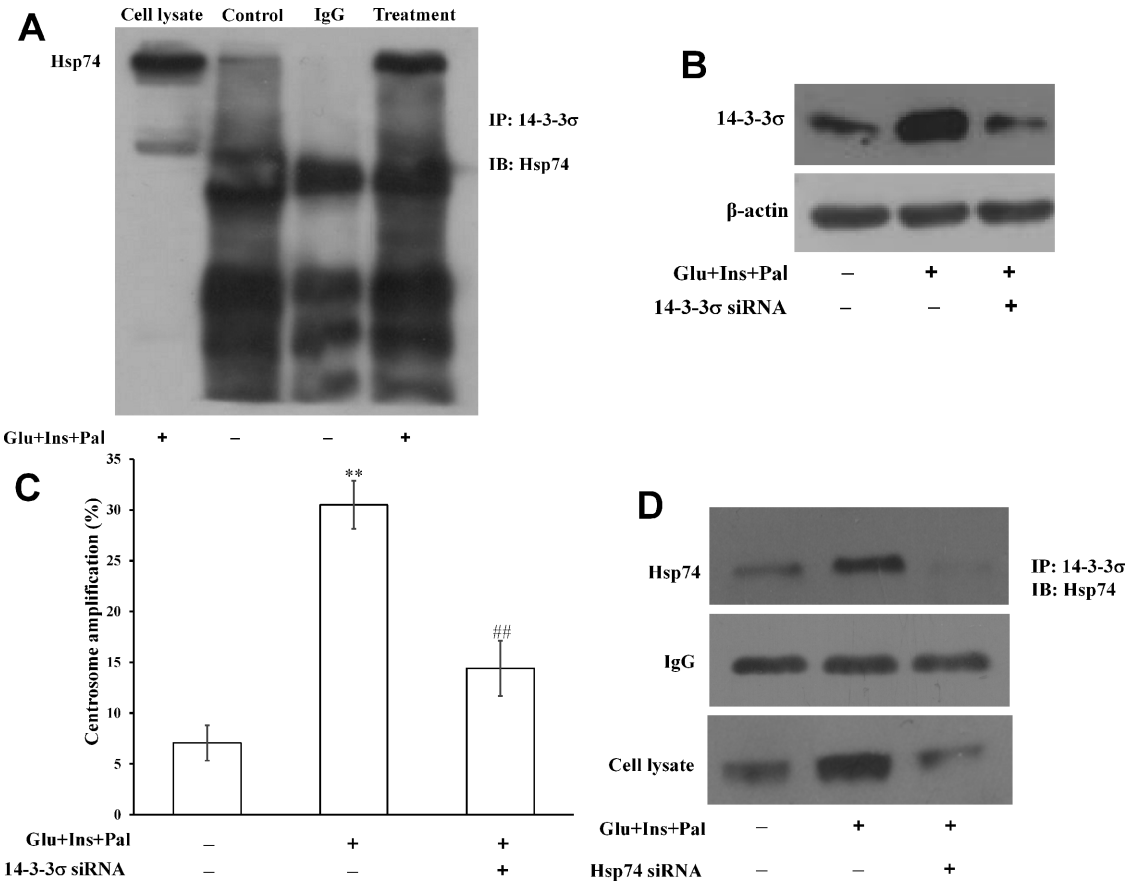

Figure 5. 14-3-3σ-Hsp74 complex is required for the centrosome amplification. Total cell lysates were used to validate the interaction between 14-3-3σ and Hsp74 by CoIP. A) CoIP of Hsp74 and 14-3-3σ. The level of Hsp74 in cell lysate was used as negative control. The Hsp74 protein was immunoprecipitated with anti-14-3-3σ antibody, and the presence of Hsp74 protein was detected by immunoblot analysis with anti-Hsp74 antibody. B) High glucose, insulin, and palmitic acid increased protein level of 14-3-3σ, which is inhibited by 14-3-3σ siRNA. C) Knockdown of 14-3-3σ downregulated the centrosome amplification. D) Knockdown of 14-3-3σ or Hsp74 disrupted the 14-3-3σ/Hsp74 complex. Glu: glucose, 15 mM; Ins: insulin, 5 nM; Pal: palmitic acid, 150 μM. $^{**}p < 0.01$, compared with that in the control group; $^{\#\#}p < 0.01$, compared with that in the samples treated with Glu, Ins, and Pal.

large aromatic side chains of ChREBP are intimately involved in both hydrogen bonding and van der Waals stacking interactions with 14-3-3.[35] In 14-3-3-Exos complex, the binding sequence of ExoS was ten residues (^{421}GLLDALDLAS^{430}). The interaction mostly relies on hydrophobic interactions and a lesser degree of electrostatic interactions.[36] In this study, we predicted the interactions of the 14-3-3σ-Hsp74 complex using molecular docking analysis. 14-3-3σ binds to Hsp74 through hydrophobic contacts, electrostatic interactions, and hydrogen bond interactions (Figure 6A,B). Compare with Mode I–III, we do not find the basic cluster of 14-3-3 residues (Lys-Arg-Arg). However, compared with 14-3-3-Exos and 14-3-3-ChREBP complex, 14-3-3σ binding to Hsp74 is also mainly through hydrophobic interactions. These data provide insight into the structural basis for the affinity binding between 14-3-3σ and Hsp74. Ideally, the binding between 14-3-3σ and Hsp74 is confirmed in vitro using purified proteins, which can specify whether phosphorylation is required for the binding or not. If yes, required phosphorylation site(s) can also be found. Mutant proteins can be created to identify the binding domain(s).

In conclusion, high glucose, insulin, and palmitic acid promote centrosome amplification by increasing expressions of 14-3-3σ and Hsp74 in HCT116 cells. The results from CoIP assay, proteomic analysis, and functional studies show the experimental treatment increase the formation of 14-3-3σ/Hsp74 complex that mediates the centrosome amplification.

Conflict of Interest

The authors declare no conflict of interest.

Acknowledgements

This study was supported by grants from Shanxi University (nos. 113533901005 and 113545017), Jiangsu Normal University and the Graduate Student Innovation Foundation of Shanxi Province (2017BY015).

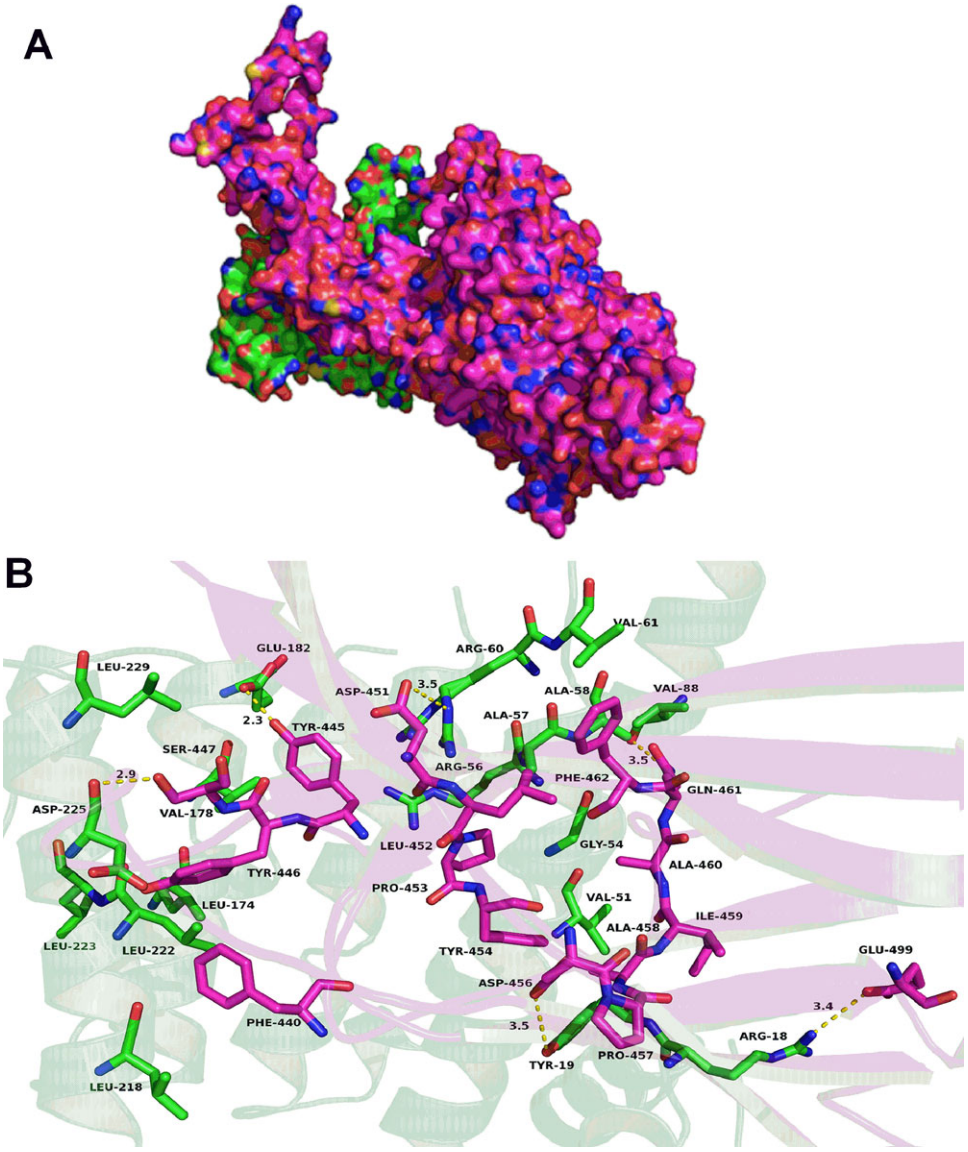

Figure 6. Homology modeling and molecular docking. A) Total view of the interaction between the 14-3-3σ and Hsp74. B) Detailed view of the interaction between the 14-3-3σ and Hsp74. Green, 14-3-3σ; rose red, Hsp74.

Keywords

14-3-3σ, Hsp74, centrosome amplification, high glucose, insulin, palmitic acid

Received: May 8, 2018
Revised: December 26, 2018
Published online: March 14, 2019

[1] F. Hua, J. J. Yu, Z. W. Hu, *Cancer lett.* **2016**, *374*, 54.
[2] B. B. Barone, H. C. Yeh, C. F. Snyder, K. S. Peairs, K. B. Stein, R. L. Derr, A. C. Wolff, F. L. Brancati, *Diabetes care* **2010**, *33*, 931.
[3] a) B. B. Barone, H. C. Yeh, C. F. Snyder, K. S. Peairs, K. B. Stein, R. L. Derr, A. C. Wolff, F. L. Brancati, *J. Am. Med. Assoc.* **2008**, *300*, 2754; b) H. C. Yeh, E. A. Platz, N. Y. Wang, K. Visvanathan, K. J. Helzlsouer, F. L. Brancati, *Diabetes care* **2012**, *35*, 113.
[4] E. A. Nigg, J. W. Raff, *Cell* **2009**, *139*, 663.
[5] E. A. Nigg, *Int. J. Cancer* **2006**, *119*, 2717.
[6] a) R. Basto, K. Brunk, T. Vinadogrova, N. Peel, A. Franz, A. Khodjakov, J. W. Raff, *Cell* **2008**, *133*, 1032; b) J. Li, J. W. Xuan, V. Khatamianfar, F. Valiyeva, M. Moussa, A. Sadek, B. B. Yang, B. J. Dong, Y. R. Huang, W. Q. Gao, *J. Pathol.* **2014**, *234*, 178; c) M. S. Levine, B. Bakker, B. Boeckx, J. Moyett, J. Lu, B. Vitre, D. C. Spierings, P. M. Lansdorp, D. W. Cleveland, D. Lambrechts, F. Foijer, A. J. Holland, *Dev. Cell* **2017**, *40*, 313.
[7] S. A. Godinho, R. Picone, M. Burute, R. Dagher, Y. Su, C. T. Leung, K. Polyak, J. S. Brugge, M. Thery, D. Pellman, *Nature* **2014**, *510*, 167.
[8] J. Y. Chan, *Int. J. Biol. Sci.* **2011**, *7*, 1122.
[9] A. Mancini, E. Imperlini, E. Nigro, C. Montagnese, A. Daniele, S. Orru, P. Buono, *Molecules* **2015**, *20*, 17339.

[10] P. Wang, Y. C. Lu, J. Wang, L. Wang, H. Yu, Y. F. Li, A. Kong, J. Chan, S. Lee, *Cell. Physiol. Biochem.* **2018**, *47*, 356.
[11] Y. C. Lu, P. Wang, J. Wang, R. Ma, S. Lee, *J. Cell. Physiol.* **2018**.
[12] a) H. Fu, R. R. Subramanian, S. C. Masters, *Annu. Rev. Pharmacol. Toxicol.* **2000**, *40*, 617; b) D. Berg, C. Holzmann, O. Riess, *Nat. Rev. Neurosci.* **2003**, *4*, 752.
[13] a) L. M. Cockrell, M. C. Puckett, E. H. Goldman, F. R. Khuri, H. Fu, *Oncogene* **2010**, *29*, 822; b) S. A. Maxwell, Z. Li, D. Jaye, S. Ballard, J. Ferrell, H. Fu, *J. Biol. Chem.* **2009**, *284*, 22379; c) V. A. Smits, R. H. Medema, *Bioch. Biophys. Acta* **2001**, *1519*, 1; d) D. V. Bulavin, Y. Higashimoto, Z. N. Demidenko, S. Meek, P. Graves, C. Phillips, H. Zhao, S. A. Moody, E. Appella, H. Piwnica-Worms, A. J. Fornace Jr, *Nat. Cell Biol.* **2003**, *5*, 545.
[14] J. Du, L. Chen, X. Luo, Y. Shen, Z. Dou, J. Shen, L. Cheng, Y. Chen, C. Li, H. Wang, X. Yao, *Front. Biosci.* **2012**, *4*, 639.
[15] A. K. Caydasi, Y. Micoogullari, B. Kurtulmus, S. Palani, G. Pereira, *Mol. Biol. Cell* **2014**, *25*, 2143.
[16] G. Tzivion, J. Avruch, *J. Biol. Chem.* **2002**, *277*, 3061.
[17] A. Mukhopadhyay, L. Sehgal, A. Bose, A. Gulvady, P. Senapati, R. Thorat, S. Basu, K. Bhatt, A. S. Hosing, R. Balyan, L. Borde, T. K. Kundu, S. N. Dalal, *Sci. Rep.* **2016**, *6*, 26580.
[18] a) S. Ko, J. Y. Kim, J. Jeong, J. E. Lee, W. I. Yang, W. H. Jung, *J. Breast Cancer* **2014**, *17*, 207; b) S. W. Kim, H. Md, M. Cho, N. H. Kim, H. Y. Choi, J. W. Han, H. J. Park, J. W. Oh, J. G. Shin, *Cell. Signal.* **2017**, *31*, 124.
[19] C. R. Brown, L. Q. Hong-Brown, S. J. Doxsey, W. J. Welch, *J. Biol. Chem.* **1996**, *271*, 833.
[20] J. Satoh, H. Onoue, K. Arima, T. Yamamura, *J. Neuropathol. Exp. Neurol.* **2005**, *64*, 858.
[21] M. Pozuelo Rubio, K. M. Geraghty, B. H. Wong, N. T. Wood, D. G. Campbell, N. Morrice, C. Mackintosh, *Biochem. J.* **2004**, *379*, 395.
[22] Y. Kaneko, T. Kimura, M. Kishishita, Y. Noda, J. Fujita, *Gene* **1997**, *189*, 19.
[23] D. M. Fathallah, D. Cherif, K. Dellagi, M. A. Arnaout, *J. Immunol.* **1993**, *151*, 810.
[24] J. Bertrand, A. Goichon, P. Chan, S. Azhar, S. Lecleire, N. Donnadieu, D. Vaudry, A. F. Cailleux, P. Dechelotte, M. Coeffier, *Amino Acids* **2014**, *46*, 1059.
[25] K. Gotoh, K. Nonoguchi, H. Higashitsuji, Y. Kaneko, T. Sakurai, Y. Sumitomo, K. Itoh, J. R. Subjeck, J. Fujita, *FEBS Lett.* **2004**, *560*, 19.
[26] T. Adachi, T. Sakurai, H. Kashida, H. Mine, S. Hagiwara, S. Matsui, K. Yoshida, N. Nishida, T. Watanabe, K. Itoh, J. Fujita, M. Kudo, *Inflamm. Bowel Dis.* **2015**, *21*, 31.
[27] P. Rafiee, M. E. Theriot, V. M. Nelson, J. Heidemann, Y. Kanaa, S. A. Horowitz, A. Rogaczewski, C. P. Johnson, I. Ali, R. Shaker, D. G. Binion, *Am. J. Physiol. Cell Physiol.* **2006**, *291*, C931.
[28] L. Chen, Y. Wang, L. Zhao, W. Chen, C. Dong, X. Zhao, X. Li, *J. Immunol. Res.* **2014**, *2014*, 492849.
[29] B. D. Clark, I. R. Brown, *Neurochem. Res.* **1987**, *12*, 819.
[30] M. Winey, E. O'Toole, *Philos. Trans. R. Soc. Lond. Ser. B Biol. Sci.* **2014**, *369*, 356.
[31] T. Obsil, V. Obsilova, *Semin. Cell Dev. Biol.* **2011**, *22*, 663.
[32] A. J. Muslin, J. W. Tanner, P. M. Allen, A. S. Shaw, *Cell* **1996**, *84*, 889.
[33] M. B. Yaffe, K. Rittinger, S. Volinia, P. R. Caron, A. Aitken, H. Leffers, S. J. Gamblin, S. J. Smerdon, L. C. Cantley, *Cell* **1997**, *91*, 961.
[34] S. Ganguly, J. L. Weller, A. Ho, P. Chemineau, B. Malpaux, D. C. Klein, *Proc. Natl. Acad. Sci. USA* **2005**, *102*, 1222.
[35] Q. Ge, N. Huang, R. M. Wynn, Y. Li, X. Du, B. Miller, H. Zhang, K. Uyeda, *J. Biol. Chem.* **2012**, *287*, 41914.
[36] C. Ottmann, L. Yasmin, M. Weyand, J. L. Veesenmeyer, M. H. Diaz, R. H. Palmer, M. S. Francis, A. R. Hauser, A. Wittinghofer, B. Hallberg, *EMBO J.* **2007**, *26*, 902.
[37] H. Seimiya, H. Sawada, Y. Muramatsu, M. Shimizu, K. Ohko, K. Yamane, T. Tsuruo, *EMBO J.* **2000**, *19*, 2652.
[38] A. Sumioka, S. Nagaishi, T. Yoshida, A. Lin, M. Miura, T. Suzuki, *J. Biol. Chem.* **2005**, *280*, 42364.